Hindawi
Advances in Materials Science and Engineering
Volume 2019, Article ID 4156176, 12 pages
https://doi.org/10.1155/2019/4156176

Research Article

Effect of Feed Rate in FSW on the Mechanical and Microstructural Properties of AA5754 Joints

Magdy M. El Rayes,[1] **Mahmoud S. Soliman**,[1] **Adel T. Abbas**,[1] **Danil Yu. Pimenov**,[2] **Ivan N. Erdakov**,[3] **and Mahmoud M. Abdel-mawla**[1]

[1]*Department of Mechanical Engineering, College of Engineering, King Saud University, P.O. Box 800, Riyadh 11421, Saudi Arabia*
[2]*Department of Automated Mechanical Engineering, South Ural State University, Lenin Prosp. 76, Chelaybinsk 454080, Russia*
[3]*Foundry Department, South Ural State University, Lenin Prosp. 76, Chelaybinsk 454080, Russia*

Correspondence should be addressed to Magdy M. El Rayes; melrayes@ksu.edu.sa

Received 7 January 2019; Revised 1 April 2019; Accepted 22 April 2019; Published 8 May 2019

Academic Editor: Jose M. Cabrera

Friction stir welding is a solid-state welding process, which is successfully applied to aluminum alloys to replace fusion welding processes. In the present work, the influence of varying the feed rate at constant rotational speed on the mechanical and microstructural properties of friction stir welded AA5754 was investigated. FSW caused dynamic recrystallization leading to microstructural changes in different zones. Electron backscattered diffraction confirmed such changes via misorientation angle and subgrain size distributions. Energy dispersive spectroscopy determined the elements present in the matrix quantitatively and their distribution through mapping. Tensile and hardness tests showed slight enhancement compared to base metal. The strain hardening exponent was used to investigate the effect of varying the feed rate on the behavior of the welded samples.

1. Introduction

Friction stir welding (FSW) is a newly introduced solid-state welding process, which was intended to replace conventional fusion welding processes that are normally accompanied by different welding defects. In the past two decades, numerous researches focused on this process since it is characterized by being energy efficient, versatile, and no localized melting and shielding gas are required. In FSW, a nonconsumable rotating tool having a shoulder and a concentric pin is brought into the opposite edges of sheets to be welded and moves along the joint. The tool provides heat arising from friction at the thickness and the workpiece surface, and mechanical stirring mixes both sides of workpiece material. This heating softens the material underneath the shoulder and surrounding the pin and thus enhances its plastic deformation leading to severe plastic deformation (SPD) hence dynamic recrystallization and consequently microstructural grain refinement [1]. Jamshidi Aval et al. [2] studied the influence of feed rate and rotational speed on the properties of AA5086 friction stir welded joints. They found that increasing tool rotational speed at a constant feed rate increases the grain size of the dynamically recrystallized grains, whereas increasing the feed rate at a constant rotational speed reduces it. In the same fashion, Hirata et al. [3] investigated the influence of the welding parameter on mechanical properties and grain size in AA5083. Similar results were obtained regarding the rotational speed with grain size, and the SZ hardness was the highest among other weldment zones. However, the tensile strength at various welding conditions was almost the same. FSW parameters of AA5083 lap joints were studied by Bisadi et al. [4], where it was reported that the welded area increased with increasing tool rotational speed, while the feed rate did not affect it. Nevertheless, it was concluded that, at lower rotational speeds, increasing feed rate enhanced the joint's mechanical properties compared to that of decreasing feed rate at higher rotational speeds. Sato et al. [5] investigated the hardness in

friction stir welds of AA1080 and 5083 and the microstructural characteristics governing it. The influence of grain boundaries on the hardness was examined in the former AA, which did not contain any second phase particles. However, the SZ consisting of recrystallized grains was harder than BM, which was related to Hall–Petch relation. The hardness profiles of the AA5083 weld were homogeneous which were related to the Orowan hardening mechanism thus indicating that the hardness profile is mainly influenced by the distribution of small particles in friction stir welds. In spite of the wide applications of AA5754 in aerospace, automotive, and marine industries, the lack of comprehensive research for studying the effect of FSW parameters on the welded joint properties was noted from the literature review. Hence, the objective of the present work is to study the effect of different feed rates (i.e., welding speeds) at constant rotational speed on the microstructural and mechanical properties of the resulting friction stir welded joint.

2. Materials and Methods

The BM used in this work was nonheat treatable AA5754-H111 with chemical analysis shown in Table 1. The treatment H111 means that the BM was strain hardened through cold working followed by a recrystallization anneal to retain some softness and ductility. The BM thickness was 6 mm and was sawed into samples ($L \times W$: 110×100 mm) by using a horizontal milling machine to produce the butt joint-square ended in which the welding line was on 110 mm length edge.

Friction stir welding runs were conducted using a Mo–W tool steel-cylindrical tool with a flat shoulder of 15 mm diameter, and a concentric square pin with an edge length of 6 mm, as in Figure 1, and 4.8 mm long.

Three feed rates (i.e., welding speeds) of 36, 70, and 140 mm/min were applied at a constant tool rotational speed of 1070 rpm, where the tool axial pressure on the workpiece was maintained constant during the entire experiments. These parameters produced sound welds in which complete intermixing between both base metals is achieved which covered the entire weldment thickness as shown macroscopically in Figure 2.

The welding setup shown elsewhere [6] was used in which the attached sheets to be joined were firmly clamped on the machine table, and the rotating tool starts welding from one end to the other. After welding, the samples were left to cool naturally in the air. Wire electrodischarge machining (EDM) was used to extract the samples for microstructure and mechanical tests where cutting was conducted perpendicular to the weld direction, and the SZ was centered within the gauge length. The dimensions of the tensile test specimens were taken according to the standard tensile test (ASTM: E08). Tensile samples were further ground from both sides to remove any scratches or dents that might have aroused during welding or preparation and to secure smooth surface finish free from any stress risers. Room temperature tensile tests were conducted using the Instron 3385H universal testing machine at a constant crosshead speed of 2 mm/min corresponding to the initial strain rate of $10^{-3}\,s^{-1}$.

Table 1: Chemical composition in wt.% of 5754-H111 aluminum alloy.

Alloying element (wt.%)	Si	Fe	Cu	Mn	Mg	Cr	Ni	Zn	Ti	Al
	0.2	0.4	0.05	0.4	3.2	0.04	0.05	0.06	0.05	Bal.

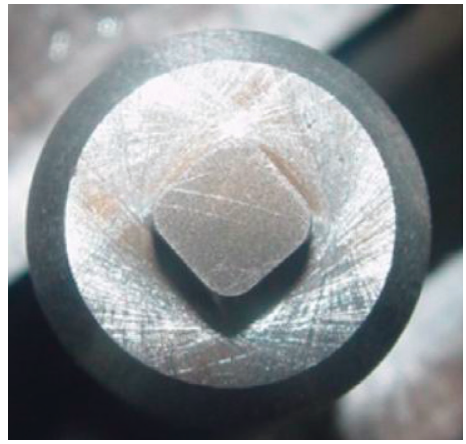

Figure 1: End view of the tool showing its shoulder and the square pin [6].

For microstructural testing of the weldments, optical microscopy (OM) and electron backscattered diffraction (EBSD) were used to study the microstructure of various weldment zones and to obtain orientation imaging grain boundary maps of the SZ microstructure, respectively. EBSD was performed using Oxford HKL system incorporated on a scanning electron microscope (SEM) JSM-6610LV JEOL. Energy dispersive spectroscopy (EDS) was conducted ten times on each sample using INCA software, which is incorporated in the SEM, and was used to determine the alloying elements present in the matrix and their distribution as well. The specimens were prepared according to the standard metallographic specimen preparation procedures including grinding, polishing, and etching. Modified Poulton's etchant composed of 2 ml HF, 3 ml HCl, 20 ml HNO_3, and 175 ml water was used to reveal the specimen's microstructure, by immersion for 10 s. The grain size was measured by a linear intercept method that was applied ten times for each microstructure to calculate the average grain size. For EBSD, the same procedure of OM was applied and then further polished using colloidal silica polishing suspension. Microhardness measurements were taken on the specimen's transverse cross section on a line located at half thickness using a Vickers microhardness tester at 500 g load and 0.5 mm incremental distance between successive indentations.

3. Results and Discussion

3.1. Microstructural Testing

3.1.1. Optical Microscopy. The microstructure obtained with all weldments was divided into three main zones, namely,

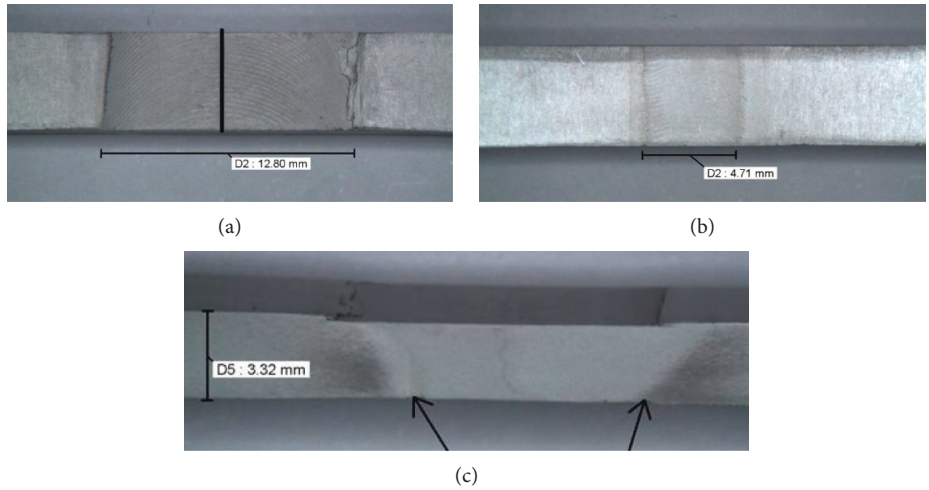

Figure 2: Macroscopic images of a friction stir welded sample showing (a) weldment top view (black line indicates the weld center), (b) weldment bottom side (root), and (c) weldment thickness.

SZ, TMAZ, and BM, as reported in all FSW literature. Figure 3 shows an optical micrograph of the BM microstructure of AA5754-H111 used in this work, where the grains are equiaxed of size around $36 \pm 2\,\mu$m. The parallel lines seen in both figures are the slip bands that aroused during cold working while manufacturing these sheets.

Within the SZ, the material undergoes SPD and also is subjected to the highest temperature compared to the neighboring zones in the weldment. Figure 4 shows the dynamically recrystallized SZ microstructures corresponding to the selected feed rates. The microstructure at the slowest feed rate; i.e., 36 mm/min, has the largest grain size of 12.6 μm, whereas it is 10.8 and 8.9 μm with the feed rates of 70 and 140 mm/min, respectively. The reason is that reducing the feed rate at constant rotational speed increases friction heating/heat input per unit length affecting the workpiece [7]. This is due to that during welding at low feed rate (i.e., 36 mm/min), the specimen spends longer time under the effect of friction heating compared to the fastest feed rate (140 mm/min). This result was also reported in previous work [8] which assumed that as the maximum temperature reached within these feed rates, static grain growth could take place after recrystallization.

Figure 5 shows an example (feed rate of 70 mm/min) to TMAZ, in which the material is plastically deformed and heated but to a lesser extent where the BM grains are elongated and rotated plastically due to the tool stirring action. Also, due to plastic deformation, slip bands/strain fields appear as parallel lines indicated by arrows as shown in Figure 5.

3.1.2. Second Phase Particles and Precipitates in the SZ. Al-Mg (5xxx series) AA is solid solution hardened systems with Mg as the primary alloying element. The maximum Mg solubility in Al (14.9 wt.% at 450°C) results in aluminum-rich solid solution; α, which determines the upper limit of solid solution strengthening in such alloy [8]. Essentially 5xxx series alloys are of the single-phase type, for example, Al_3Mg_2, $A1_6$ (Fe, Mn) [9] such as Al_6Mn, $A1_3Fe$, and α-Al (Fe, Mn, Si) which are dispersed as second phase particles within the aluminum matrix [8, 10]. The Al_3Mg_2 phase melts at 450°C [11] and forms both intergranular as well as at the grain boundaries causing preferential Mg depletion in the grain boundary [8, 12]. Al_6Mn is an intermetallic phase that has a melting temperature of 705°C [11] which is higher than the solidus temperature of AA5754 thus making it effective particles type to prevent grain growth at high temperatures [8]. Energy dispersive spectroscopy (EDS) was used to identify the elements present in the matrix where Al, Mg, Si, Mn, and Fe which were found to be present in the entire matrix of the stir zones corresponding to the three feed rates. Figure 6 shows an example of EDS analysis of the SZ of the sample welded at 140 mm/min. The elemental analysis presented in this figure is almost identical to that presented in Table 1.

To further investigate the elemental distribution in the microscale, EDS elemental mapping was taken within the same zone of EDS quantitative analysis, presented in Figure 6. Results revealed and confirmed the presence of such elements within the SZ matrix, as shown in Figure 7. The EDS elemental map evidences the homogeneous distribution of all elements found in the quantitative results.

EDS was further conducted at higher magnification, for at least five times on the particles to solely identify their elemental composition. Figures 8(a) and 8(b) show the results obtained from the particles present in BM and SZ, respectively. Compared to the chemical composition presented in Figure 6, it was noted that particles in both locations (i.e., BM and SZ) are second phase particles that are composed of higher weight percents of Mg and Si and lower Al. The reason for the difference regarding the SZ as compared to the BM may be due to the friction heating and fragmentation of these particles, which favour the dissolution and diffusion of such elements into the matrix.

Figure 9 shows a generalized view at a low magnification of polished and unetched weldments for the particles distribution found in BM and SZ of an example sample welded at 70 mm/min. The BM possessed a combination of the large

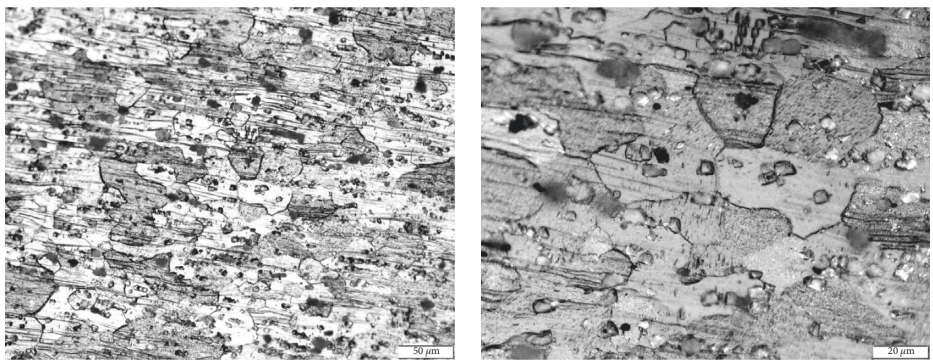

(a) (b)

Figure 3: Optical micrographs of BM of AA5754 at different magnifications for the same location.

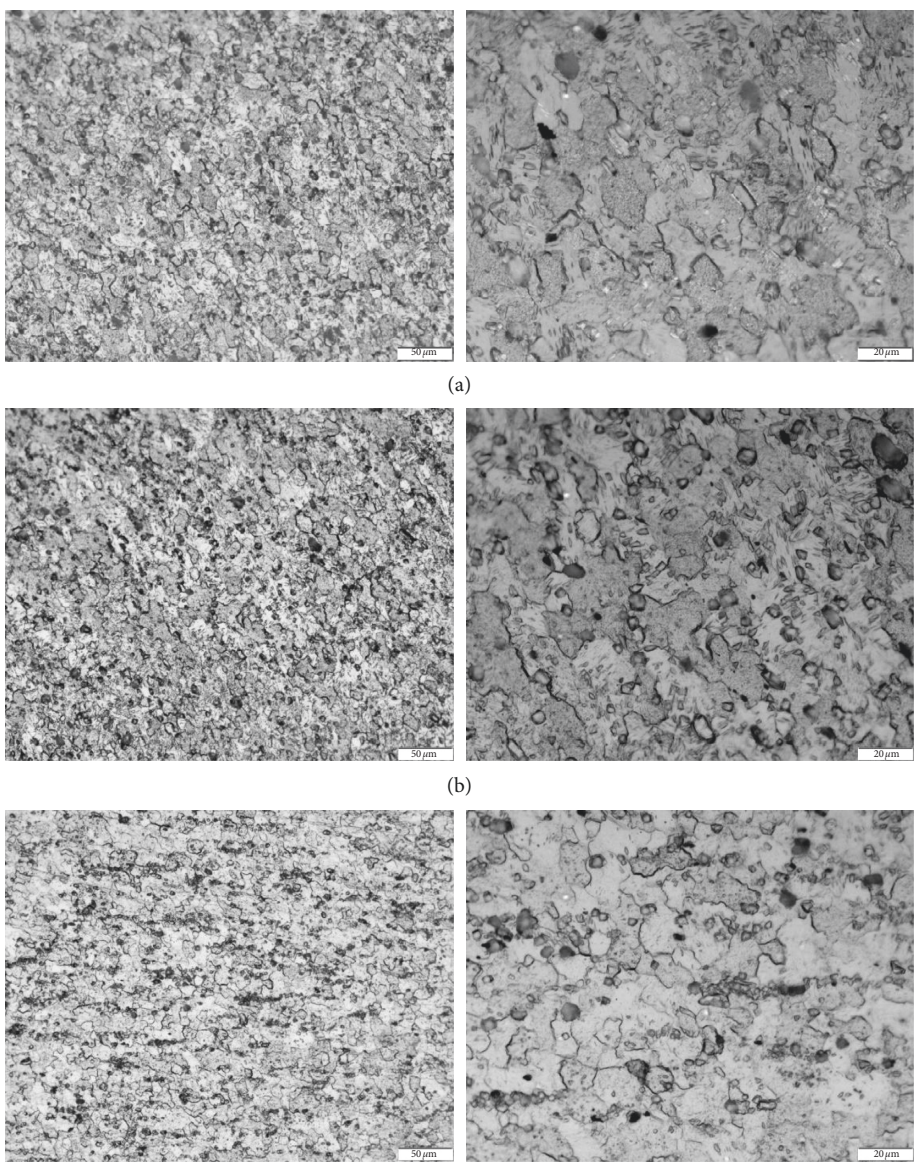

(a)

(b)

(c)

Figure 4: The microstructure of the stir zone (SZ) for friction stir welded samples at 1070 rpm and three feed rates: (a) 36 mm/min; (b) 70 mm/min; (c) 140 mm/min. Left and right columns correspond to the same location but different magnifications.

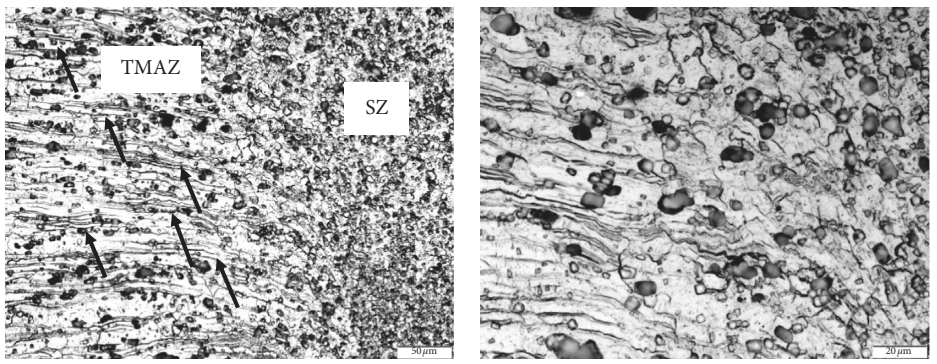

(a) (b)

Figure 5: Optical micrographs of TMAZ of the sample welded at 70 mm/min, at different magnifications.

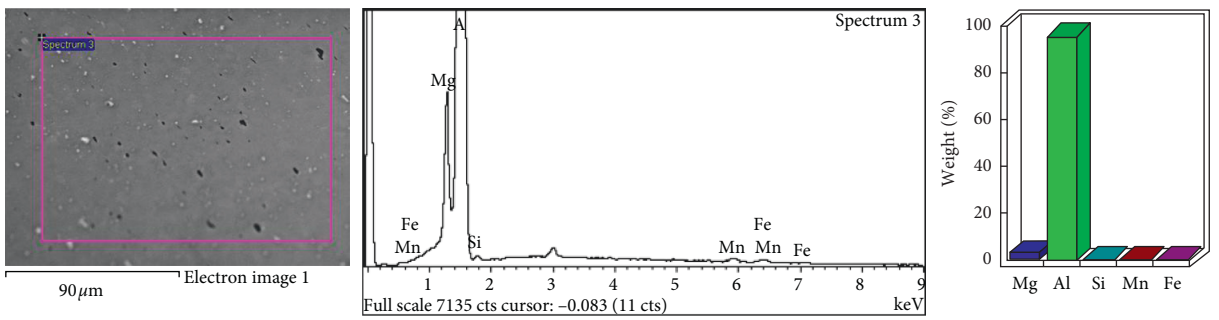

Al: 95.76; Mg: 3.11; Si: 0.27; Mn: 0.43; Fe: 0.43. wt. (%)

Figure 6: Example of EDS analysis at SZ of sample welded at 140 mm/min. (a) Scanned area; (b) element histogram; (c) quantitative EDS results.

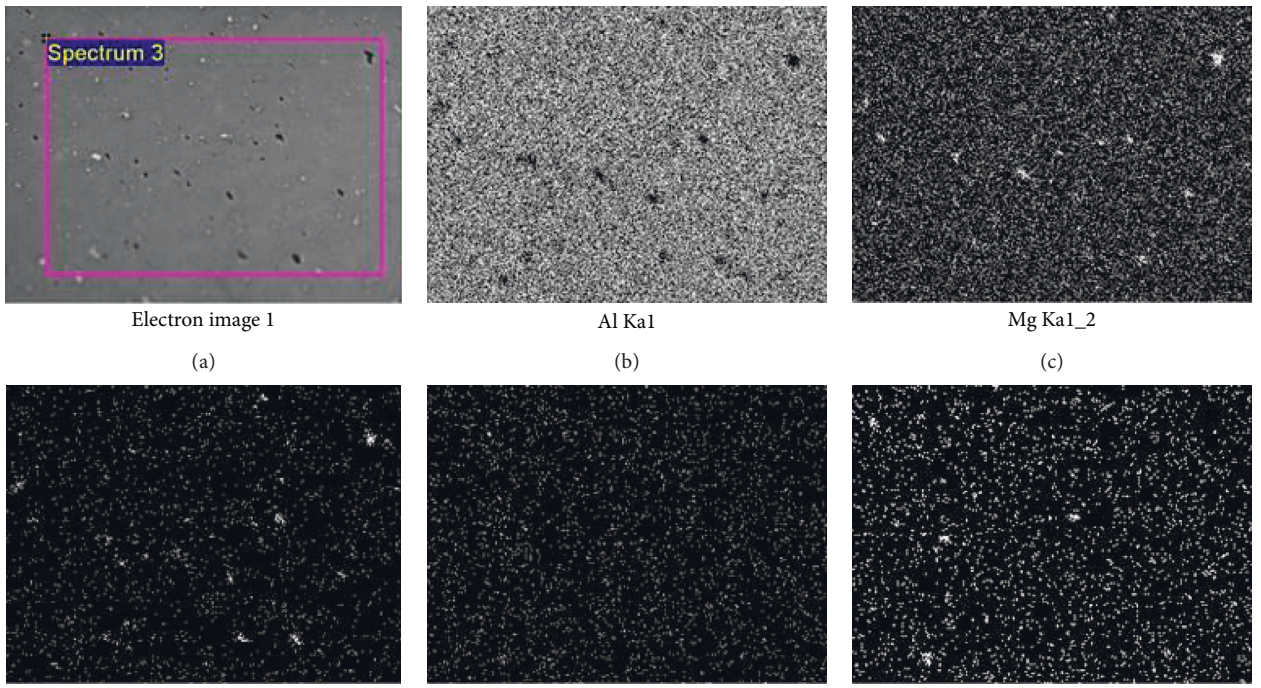

(a) (b) (c)

(d) (e) (f)

Figure 7: Low magnification observations and EDS elemental mapping analysis of the SZ of the sample welded at 140 mm/min showing the distribution of various elements. (a) Scanned area; (b) Al; (c) Mg; (d) Si; (e) Mn; (f) Fe.

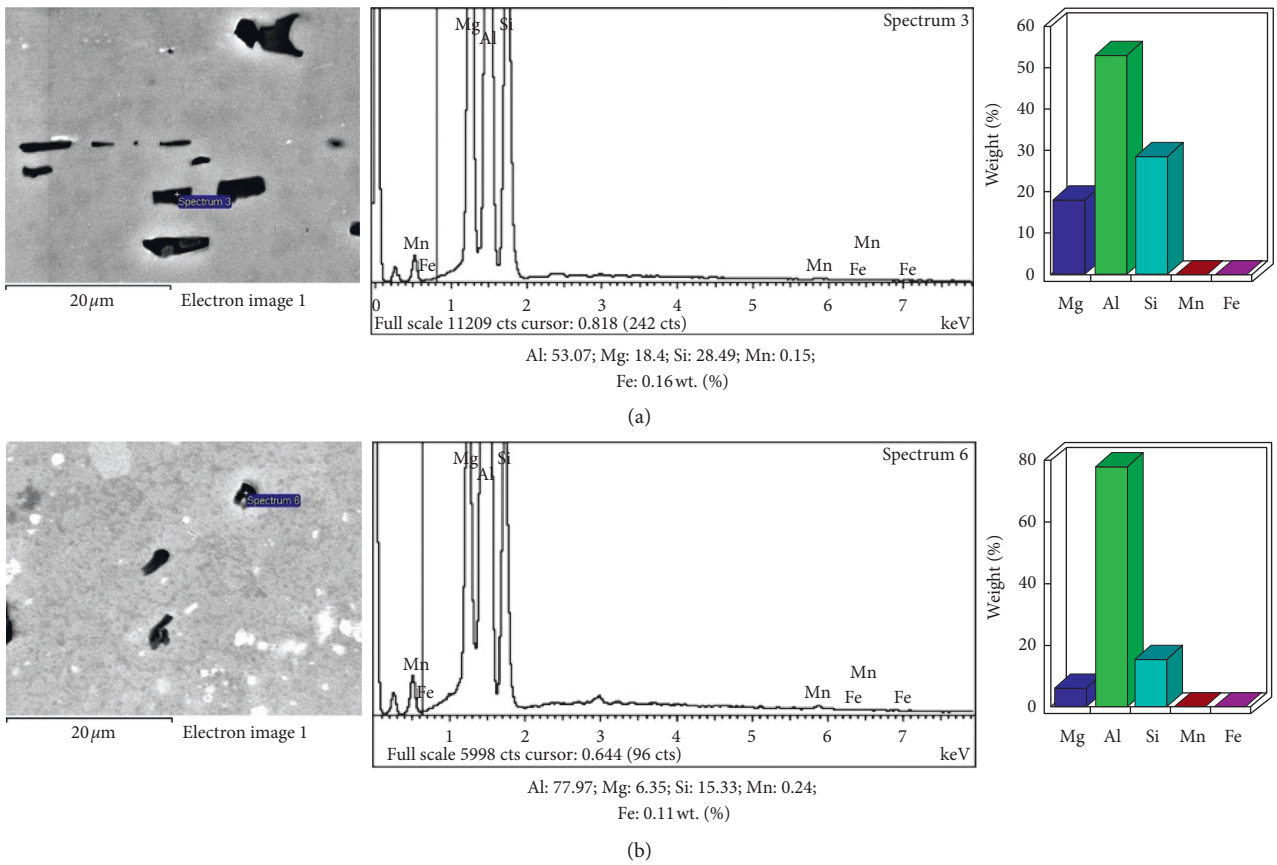

Figure 8: High magnification EDS elemental analysis of the second phase particles present in (a) base metal and (b) stir zone.

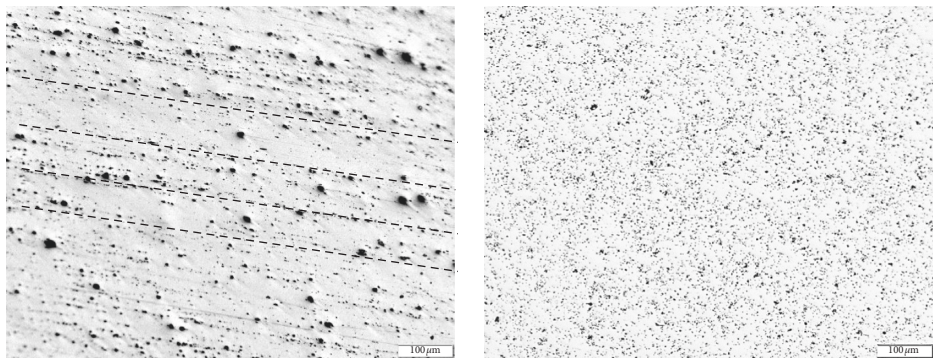

(a) (b)

Figure 9: Comparison between morphology and population of precipitates found in (a) BM and (b) SZ.

and small size of particles gathered in the form of parallel bands shown by straight dotted lines in Figure 9(a). These bands might be due to annealing during production where they cluster/segregate alternately in bands and absent in the neighbor one. Figure 9(b), on the contrary, shows the small-sized and homogeneously distributed particles within the entire SZ. This is due to the stirring action of the FSW tool, which caused fragmentation of them during welding.

Higher magnification was used to better visualize the population and morphology of particles present in BM and SZ of the three welded samples, as shown in Figure 10. The population/area fraction of these particles concerning the matrix was measured using a software attached to the optical microscope, where five measurements were taken for each location at the SZ center. This software measures the dark spot areas compared to that of the light matrix. The difference between particles morphology and population of particles in the BM and SZ is seen in Figure 10. Generally, the particles in the SZ are mechanically fragmented/fractured, smeared, and mixed to different geometries because of the tool stirring [13]. In the BM, on the contrary, the particles have a larger size (coarse) when compared to that found in other zones, assume almost round shape, and heterogeneously distributed within the aluminum matrix giving area fraction of $14.4 \pm 1.4\%$. In

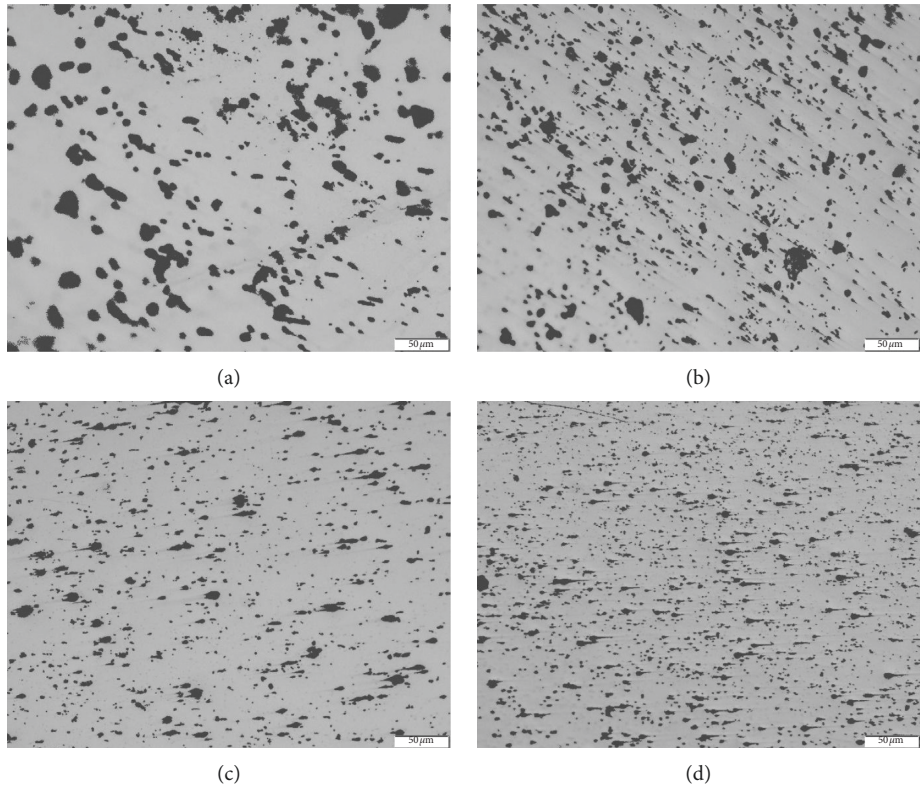

(a) (b)

(c) (d)

Figure 10: Particle morphology and population measured at (a) BM (14.4%) and SZ for samples welded with different feed rates: (b) 36 mm/min (12.1%), (c) 70 mm/min (9.54), and (d) 140 mm/min (7.73%).

the SZ, the particles were fragmented and became much smaller and still assume round shape but more homogenously distributed within the matrix. This is because of the stirring action of the tool pin combined with the workpiece advancement during welding, as reported earlier in FSW of 5xxx AA series [5, 9, 13–15]. Figure 10 also shows that increasing the feed rate reduces the particles size and their density leading to smaller area fraction % (i.e., 12.1 ± 1.4, 9.54 ± 1.1, and 7.73 ± 0.7% corresponding to 36, 70, and 140 mm/min, respectively) due to fragmentation and redistribution within the entire matrix. This result is similarly reported in different earlier publications [10, 11, 13, 16, 17].

3.1.3. EBSD Microstructural Analysis. Figures 11(a)–11(c) show orientation imaging grain boundary maps and their corresponding histogram for the misorientation angle and subgrain size distributions taken at the SZ of the three samples investigated. As stated above, the sample welded at 36 mm/min is exposed to the highest heat input among other samples welded at higher speeds. This increased heating and natural cooling leave the grain size of dynamically recrystallized grains in the SZ of 9.4, 5.7, and 5.2 μm corresponding to feed rates of 36, 70, and 140 mm/min, respectively, as presented in Figure 11.

It is already confirmed in all literature that FSW exhibits localized SPD within the SZ, leading to dynamic recrystallization and hence grain refinement with equiaxed microstructure. Therefore, it can be stated that exposure to the highest temperature and thus the highest deformation occur at the SZ compared to the neighboring zones. On the contrary, decreasing the feed rate increases plastic deformation which in turn increases the average misorientation angle of the evolved microstructure. This can be noted in Figure 11 for average misorientation angles of 26°, 24°, and 21° at feed rates of 36, 70, and 140 mm/min, respectively. Also, the application of SPD normally leads to the evolution of large subgrain boundaries, which is expressed as a percentage of low-angle grain boundaries (LAGBs).

Nevertheless, the highest heat input corresponding to the feed rate of 36 mm/min causes more recovery to the microstructure, which can be depicted from three microstructural features noted in Figure 11. They are, namely, first, the lowest LAGB (31°); second, highest high-angle grain boundary (HAGB) (69°); and third, the largest average subgrain size; i.e., 9.4 μm, proving that a greater extent of recovery has occurred with the lowest feed rate. Here, it is worth comparing the grain size obtained from OM with EBSD, which is found that the grain size obtained from the latter is smaller than the former. This is because backscattered electrons in EBSD are more sensitive to surface details than light in OM. In addition, the chemical etching produces steps at the grain boundaries, which do not provide well-defined grain structure that can be resolved in the light microscope and finally grain boundary precipitates may delineate the grain boundaries upon chemical etching, which makes it difficult or impossible to produce any grain contrast as reported by Gao et al. [18].

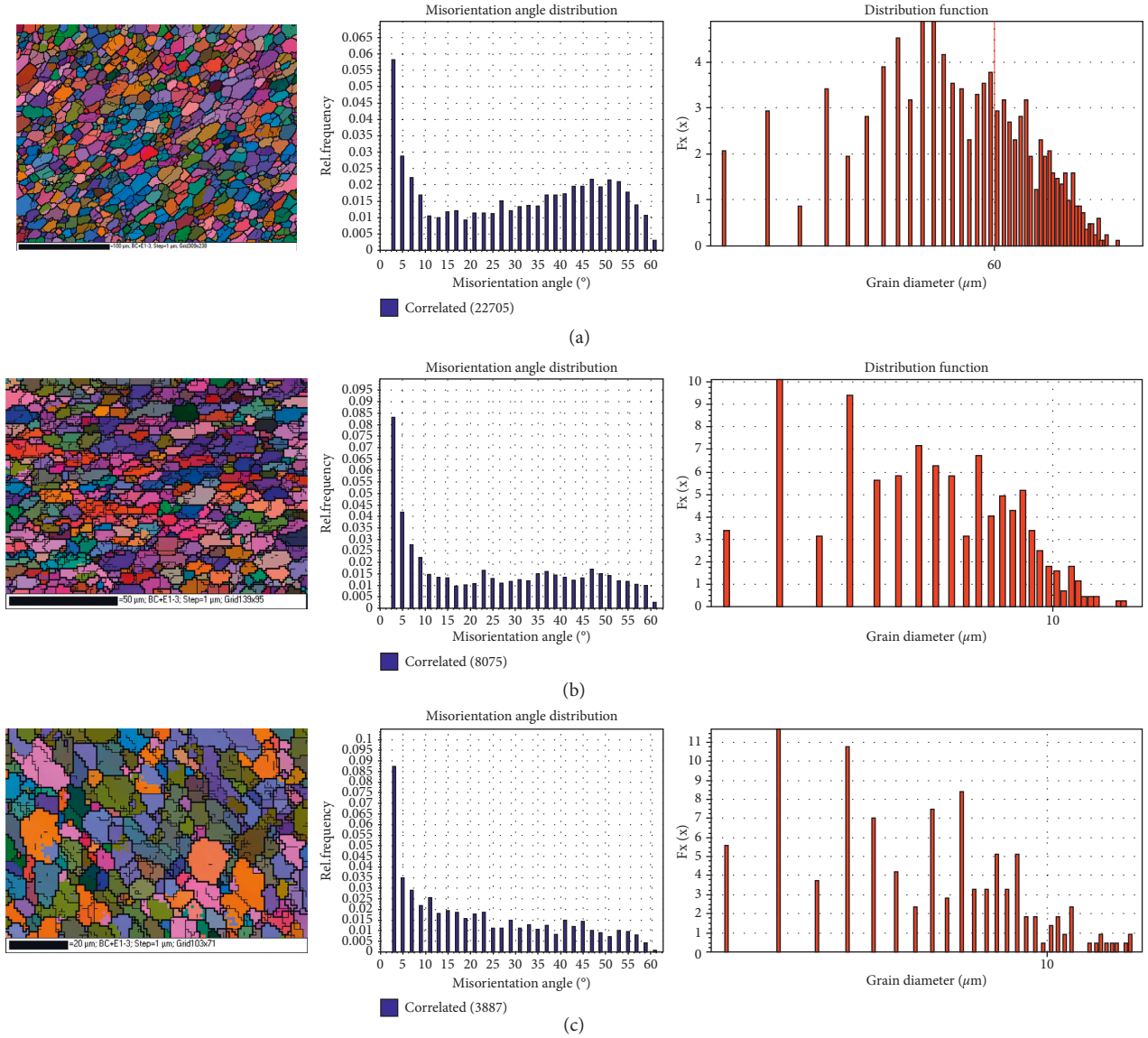

Figure 11: Orientation imaging grain boundary maps (left column), their corresponding histogram for the misorientation angle distribution (middle column), and subgrain size distributions (right column) for friction stir welded joints welded at 1070 rpm and different feed rates: (a) 36 mm/min; (b) 70 mm/min; (c) 140 mm/min. Average misorientation angle: (a) 26°; LAGB: 31%; HAGB: 69%; (b) 24°; LAGB: 44%; HAGB: 56%; (c) 21°; LAGB: 48%; HAGB: 52%.

Furthermore, SPD contributes to high strain energy to subgrain boundary microstructures thus provideing a driving force for recovery and recrystallization during higher/longer heating. Hence, low-angle, low-energy boundaries are reduced by recovery mechanisms, whereas, high-angle, high-energy boundaries are rearranged by grain coarsening mechanisms. Here, it should be noted that the misorientation angle distribution histogram (Mackenzie plot) shown in Figure 11(a) indicates full recrystallization in the SZ, whereas, in Figures 11(b) and 11(c), partial recrystallization is deduced in spite of the fact that complete recrystallization and consequent grain refinement was observed in the OM tests.

3.2. Mechanical Properties. As mentioned above, FSW results in significant microstructural changes within and next to the SZ. This probably leads to variations in the mechanical properties of the weldments.

3.2.1. Hardness Distribution. The Vickers microhardness measurements were conducted on the traverse cross section of the weldment at a line inscribed at its half thickness. Generally, the hardness profile across all weldments gave a similar trend in which the hardness is maximum at the SZ and is then gradually reduced towards the BM as in Figure 12. This profile is similar to that found in the earlier literature [4, 10, 19–22] that applied FSW on AA5xxx series alloys. The reason why the SZ is hardest compared to the BM is because of the finer grain size than in the BM as mentioned above in the metallographic section. Since the grain boundaries are one of

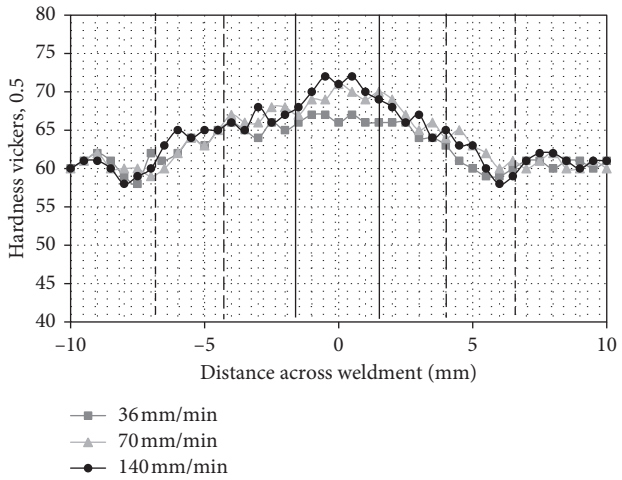

Figure 12: Hardness distribution across weldments welded at different feed rates.

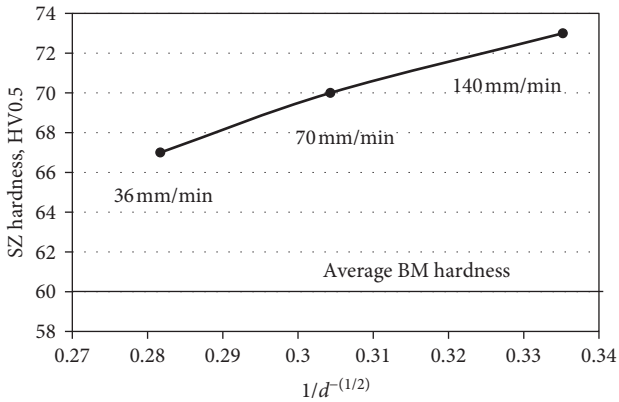

Figure 13: The relation between average SZ hardness and average SZ grain size according to the Hall–Petch relation. Note: the horizontal line represents the average hardness of the BM.

the major obstacles to the slip of dislocations, smaller grain size would have a higher resistance to the localized plastic deformation giving rise to strength and consequently hardness during the penetration of the microhardness test indenter [23].

Furthermore, the presence of particles with homogeneous distribution and small size, which was noted in the SZ, as well as the greater postweld natural aging, maybe also other reasons for the higher hardness in the SZ compared to that in the BM. A similar result is reported in the earlier work [13, 15, 22]. The average hardness values of the three samples measured in the SZ were 67 ± 1, 70 ± 1, and 73 ± 2 HV0.5 corresponding to 36, 70, and 140 mm/min respectively. Although this trend indicates that SZ hardness increases with increasing feed rate as reported earlier [8], these values are close to each other. Thus it can be stated that there is a minor effect of varying the feed rate on SZ hardness.

Nevertheless, because of the higher heat input and temperature exposure occurring with a low feed rate of 36 mm/min compared to higher ones, this consequently promotes recovery and reduces the fraction of subgrain boundaries; i.e., LAGBs 31° all of which reduce the SZ hardness. Grain size is another probable reason for hardness variation within the SZ. As already known in grain boundary strengthening, dislocation propagation is impeded and hindered by grain boundaries; hence, the yield strength (YS) of the material is increased. Decreasing the grain size increases the amount of applied stress necessary to move a dislocation across the grain boundary [13]. Therefore, the inverse relation between grain size and YS, demonstrated by Hall–Petch, indicates that smaller grain size create more obstacles to the dislocation movement and hence strengthens the material as reported in [13]. The relationship between hardness and the SZ grain size $d^{-1/2}$ [3] is presented in Figure 13 showing the relationship which mostly yielded a straight line.

In the TMAZ, the hardness is then reduced in the TMAZ, which was subjected to less plastic deformation hence incomplete dynamic recrystallization. Another zone appeared next to the TMAZ, which possesses minimum hardness between 57 and 60 HV0.5. Although this zone was not distinguished microstructurally, it can be considered as the heat affected zone (HAZ), beyond which the hardness increases towards the unaffected BM giving the value of around 60 HV0.5. It was reported [24] that the difficulty of distinguishing the HAZ indicates that this zone did not experience any plastic deformation but is subjected only to the weld thermal cycle [13].

3.2.2. Tensile Properties. The engineering stress-strain curves corresponding to the three feed rates along with that of the BM are shown in Figure 14. FSW slightly strengthens the weldments because of the refined-dynamically recrystallized grains within the SZ. This consequently led to an increase in the ultimate tensile (UTS) and yield (YS) strengths and reduction in ductility compared to BM. The variation of the feed rate has a minor influence on both the UTS and YS and also ductility. However, it is worth mentioning that the gauge length of the tensile samples included SZ, TMAZ, HAZ, and BM. Increasing the feed rate is accompanied by a slight increase in UTS and a decrease in ductility, whereas the YS is almost unchanged. On the contrary, the effect of varying the feed rate on the engineering stress-strain plots is minimal where the UTS and the YS are almost similar, whereas, nevertheless, ductility is highest with the slowest feed rate 36 mm/min. This may be due to the relatively higher heat input accompanying the slowest feed rate, which results in reduced strain hardening behavior, a greater extent of recovery and grain coarsening all of which promote ductility.

To investigate the influence varying feed rate on the resulting strain hardening behavior of the welded samples, true stress-true strain relation was plotted on a log-log scale as in Figure 15. This figure shows that the sample corresponding to 36 mm/min possessed highest strain hardening exponent $n = 0.324$ when compared to that of 70 and 140 mm/min having values of 0.3053 and 0.2977, respectively. The reason for this result may be due to the highest particles density present in the SZ of the sample

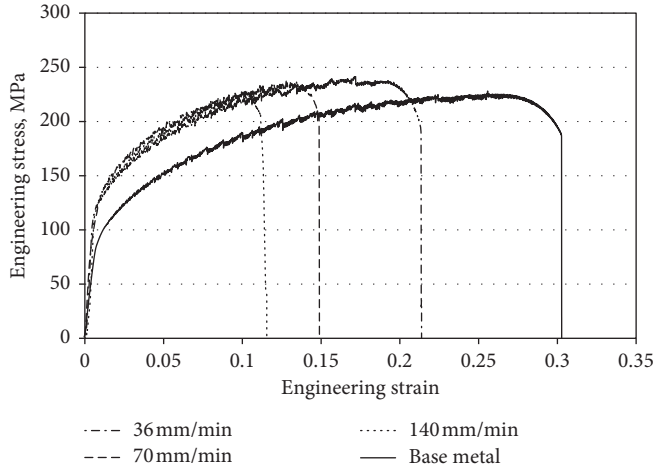

Figure 14: Engineering stress-strain curves of BM and friction stir welded joints of AA5754.

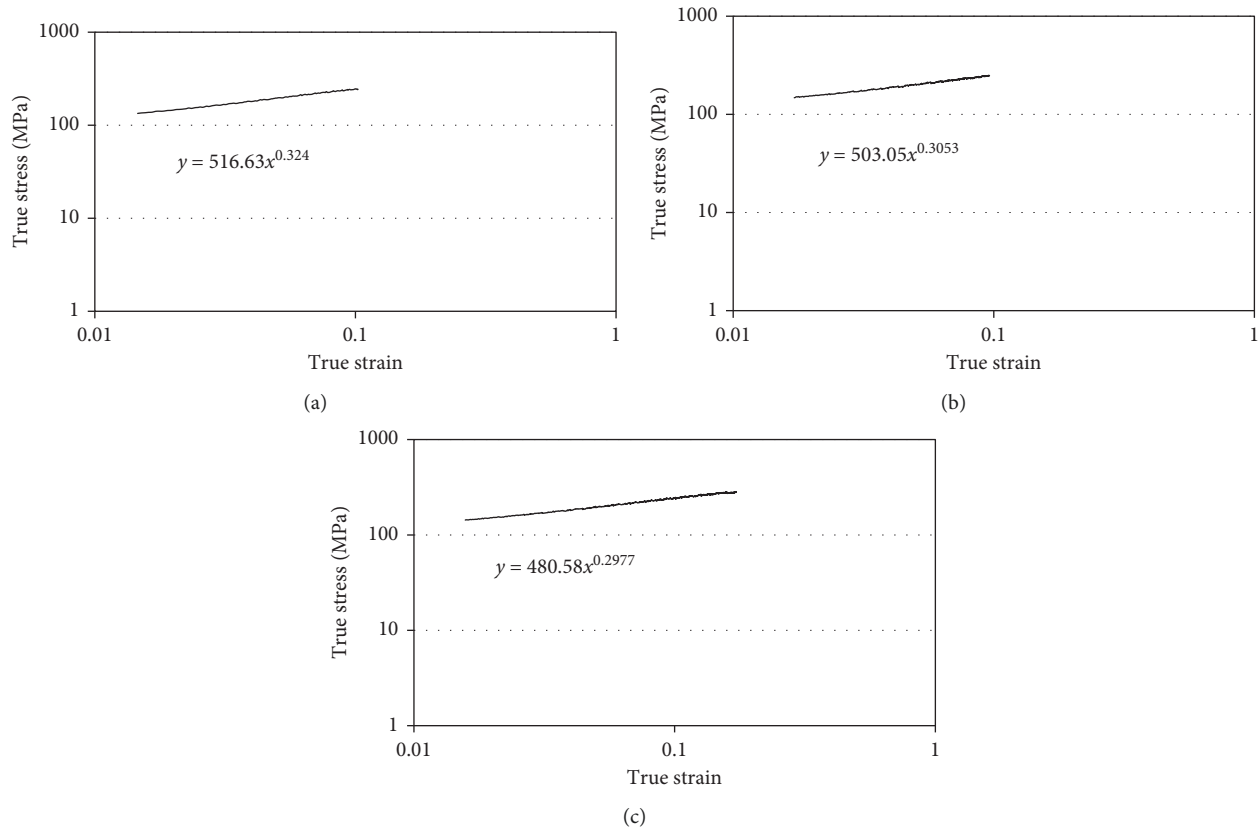

Figure 15: True stress-true strain plot log-log scale of FSW samples welded at different feed rates: (a) 36 mm/min; (b) 70 mm/min; (c) 140 mm/min.

welded at 36 mm/min in comparison with other feed rates. Bauri and Yadav [26] reported the effect of particles in the nonheat treatable AA on the strength and strain hardening behaviors. Higher amounts of particles lead to higher pinning effect within the grains and on their boundaries thus leading to more resistance to further plastic deformation hence higher stain hardening. Another reason may also play a role in increasing the strain hardening is the grain size. Earlier findings [26] indicated that dislocation annihilation rate is low in coarser grained structures due to the larger distance between boundaries thus promoting more strain hardening with these grains. This is reflected on the higher strain hardening exponent with coarser grain size.

4. Conclusions

The influence of increasing the feed rate at constant rotational speed on microstructural characteristics and mechanical

properties in FSW of AA5754 was investigated in this study. Increasing the feed rate is accompanied by reduction in the friction heating and thus reduction in the grain and subgrain sizes as well as a reduction in the extent of recovery in the SZ. Furthermore, it reduces the average misorientation angle, whereas it increases the low-angle grain boundaries. Increasing the feed rate also increases the fragmentation and homogenizes the second phase particles within the SZ matrix and therefore reduces the values of ductility and strain hardening exponent of the joint. In addition, it enhances the YS and UTS of the weldments compared to that of BM and also slightly increases the SZ hardness.

Data Availability

The data used to support the findings of this study are available from the corresponding author upon request.

Conflicts of Interest

The authors declare that they have no conflicts of interest.

Acknowledgments

The authors extend their appreciation to the Deanship of Scientific Research at King Saud University for funding this work through research group (no. RG-1439-020). The research was also supported through Act 211 of the Government of the Russian Federation under contract no. 02.A03.21.0011.

References

[1] R. S. Mishra and Z. Y. Ma, "Friction stir welding and processing," *Materials Science and Engineering: R: Reports*, vol. 50, no. 1-2, pp. 1–78, 2005.

[2] H. Jamshidi Aval and A. Loureiro, "Effect of welding parameters on microstructure, mechanical properties and residual stress fields of friction stir welds on AA5086," *Metallic Materials*, vol. 53, no. 1, pp. 51–58, 2015.

[3] T. Hirata, T. Oguri, H. Hagino et al., "Influence of friction stir welding parameters on grain size and formability in 5083 aluminum alloy," *Materials Science and Engineering: A*, vol. 456, no. 1-2, pp. 344–349, 2007.

[4] H. Bisadi, M. Tour Sangsaraki, and A. Tavakoli, "The influence of process parameters on microstructure and mechanical properties of friction stir welded Al 5083 alloy lap joint," *American Journal of Materials Science*, vol. 1, no. 2, pp. 93–97, 2012.

[5] Y. S. Sato, S. H. C. Park, and H. Kokawa, "Microstructural factors governing hardness in friction-stir welds of solid-solution-hardened Al alloys," *Metallurgical and Materials Transactions A*, vol. 32, no. 12, pp. 3033–3042, 2001.

[6] E. A. El-Danaf and M. M. El-Rayes, "Microstructure and mechanical properties of friction stir welded 6082 AA in as welded and post weld heat treated conditions," *Materials & Design*, vol. 46, pp. 561–572, 2013.

[7] T. Sakthivel, G. S. Sengar, and J. Mukhopadhyay, "Effect of welding speed on microstructure and mechanical properties of friction-stir-welded aluminum," *International Journal of Advanced Manufacturing Technology*, vol. 43, no. 5-6, pp. 468–473, 2009.

[8] A. Tronci, R. McKenzie, R. M. Leal, and D. M. Rodrigues, "Microstructural and mechanical characterisation of 5XXX-H111 friction stir welded tailored blanks," *Science and Technology of Welding and Joining*, vol. 16, no. 5, pp. 433–439, 2011.

[9] R. S. Mishra, P. S. De, and N. Kumar, "FSW of aluminum alloys," in *Friction Stir Welding and Processing: Science and Engineering*, R. S. Mishra, P. S. De, and N. Kumar, Eds., pp. 109–148, Springer International Publishing, Cham, Switzerland, 2014.

[10] Y. Chen, H. Ding, Z. Cai, J. Zhao, and J. Li, "Microstructural and mechanical characterization of a dissimilar friction stir-welded AA5083-AA7B04 butt joint," *Journal of Materials Engineering and Performance*, vol. 26, no. 2, pp. 530–539, 2017.

[11] M. M. Z. Ahmed, S. Ataya, M. M. El-Sayed Seleman, H. R. Ammar, and E. Ahmed, "Friction stir welding of similar and dissimilar AA7075 and AA5083," *Journal of Materials Processing Technology*, vol. 242, pp. 77–91, 2017.

[12] A. Gerlich, M. Yamamoto, and T. H. North, "Strain rates and grain growth in Al 5754 and Al 6061 friction stir spot welds," *Metallurgical and Materials Transactions A*, vol. 38, no. 6, pp. 1291–1302, 2007.

[13] R. Goswami, G. Spanos, P. S. Pao, and R. L. Holtz, "Precipitation behavior of the *ß* phase in Al-5083," *Materials Science and Engineering: A*, vol. 527, no. 4-5, pp. 1089–1095, 2010.

[14] R. Moshwan, F. Yusof, M. A. Hassan, and S. M. Rahmat, "Effect of tool rotational speed on force generation, microstructure and mechanical properties of friction stir welded Al–Mg–Cr–Mn (AA 5052-O) alloy," *Materials & Design (1980–2015)*, vol. 66, pp. 118–128, 2015.

[15] M. A. García-Bernal, R. S. Mishra, R. Verma, and D. Hernández-Silva, "Influence of friction stir processing tool design on microstructure and superplastic behavior of Al-Mg alloys," *Materials Science and Engineering: A*, vol. 670, pp. 9–16, 2016.

[16] L.-E. Svensson, L. Karlsson, H. Larsson, B. Karlsson, M. Fazzini, and J. Karlsson, "Microstructure and mechanical properties of friction stir welded aluminium alloys with special reference to AA 5083 and AA 6082," *Science and Technology of Welding and Joining*, vol. 5, no. 5, pp. 285–296, 2000.

[17] T. Chen, W.-B. Lin, and C.-M. Hung, "Microstructure in the FSW butt joint of aluminum alloy AA5083," in *Proceedings of the 2012 Annual Conference on Experimental and Applied Mechanics*, C. E. Ventura, W. C. Crone, and C. Furlong, Eds., vol. 4, pp. 143–147, Springer New York, Costa Mesa, CA, USA, June 2013.

[18] Q. Zhao, B. Holmedal, and Y. Li, "Influence of dispersoids on microstructure evolution and work hardening of aluminium alloys during tension and cold rolling," *Philosophical Magazine*, vol. 93, no. 22, pp. 2995–3011, 2013.

[19] N. Gao, S. C. Wang, H. S. Ubhi, and M. J. Starink, "A comparison of grain size determination by light microscopy and EBSD analysis," *Journal of Materials Science*, vol. 40, no. 18, pp. 4971–4974, 2005.

[20] E. A. El-Danaf, M. M. El-Rayes, and M. S. Soliman, "Friction stir processing: an effective technique to refine grain structure and enhance ductility," *Materials & Design*, vol. 31, no. 3, pp. 1231–1236, 2010.

[21] J. S. Jesus, M. Gruppelaar, J. M. Costa, A. Loureiro, and J. A. M. Ferreira, "Effect of geometrical parameters on friction stir welding of AA 5083-H111 T-joints," *Procedia Structural Integrity*, vol. 1, pp. 242–248, 2016.

[22] S. Amini, M. R. Amiri, and A. Barani, "Investigation of the effect of tool geometry on friction stir welding of 5083-O aluminum alloy," *International Journal of Advanced Manufacturing Technology*, vol. 76, no. 1–4, pp. 255–261, 2015.

[23] L. Serio, D. Palumbo, L. De Filippis, U. Galietti, and A. Ludovico, "Effect of friction stir process parameters on the mechanical and thermal behavior of 5754-H111 aluminum plates," *Materials*, vol. 9, no. 3, p. 122, 2016.

[24] S. H. Chowdhury, D. L. Chen, S. D. Bhole, X. Cao, and P. Wanjara, "Lap shear strength and fatigue life of friction stir spot welded AZ31 magnesium and 5754 aluminum alloys," *Materials Science and Engineering: A*, vol. 556, pp. 500–509, 2012.

[25] N. T. Kumbhar, S. K. Sahoo, I. Samajdar, G. K. Dey, and K. Bhanumurthy, "Microstructure and microtextural studies of friction stir welded aluminium alloy 5052," *Materials & Design*, vol. 32, no. 3, pp. 1657–1666, 2011.

[26] R. Bauri and D. Yadav, *Metal Matrix Composites by Friction Stir Processing*, Department of Metallurgical and Materials Engineering, India Institute of Technology, Library of Congress, Chennai, India, 2018, ISBN: 978-0-12-813729-1.